Click Here for Full Article

Electron loss rates from the outer radiation belt caused by the filling of the outer plasmasphere: The calm before the storm

Joseph E. Borovsky[1] and Michael H. Denton[2]

[1] Measurements from seven spacecraft in geosynchronous orbit are analyzed to determine the decay rate of the number density of the outer electron radiation belt prior to the onset of high-speed-stream-driven geomagnetic storms. Superposed-data analysis is used with a collection of 124 storms. When there is a calm before the storm, the electron number density decays exponentially before the storm with a 3.4-day e-folding time: beginning about 4 days before storm onset, the density decreases from $\sim 4 \times 10^{-4}$ cm^{-3} to $\sim 1 \times 10^{-4}$ cm^{-3}. When there is not a calm before the storm, the number density decay is very small. The decay in the number density of radiation belt electrons is believed to be caused by pitch angle scattering of electrons into the atmospheric loss cone as the outer plasmasphere fills during the calms. This is confirmed by separately measuring the density decay rate for times when the outer plasmasphere is present or absent. While the radiation belt electron density decreases, the temperature of the electron radiation belt holds approximately constant, indicating that the electron precipitation occurs equally at all energies. Along with the number density decay, the pressure of the outer electron radiation belt decays, and the specific entropy increases. From the measured decay rates, the electron flux to the atmosphere is calculated, and that flux is 3 orders of magnitude less than thermal fluxes in the magnetosphere, indicating that the radiation belt pitch angle scattering is 3 orders weaker than strong diffusion. Energy fluxes into the atmosphere are calculated and found to be insufficient to produce visible airglow.

1. Introduction

[2] The outer portions of the plasmasphere build up and drain away with changes in geomagnetic activity [e.g., *Chappell et al.*, 1970; *Carpenter et al.*, 1993; *Elphic et al.*, 1997; *Sandel and Denton*, 2007], the buildup occurring when geomagnetic activity is weak and the drainage occurring when geomagnetic activity strengthens. During recurrent high-speed-stream-driven storms, the outer plasmasphere goes through an episodic cycle of slowly building up in density and then rapidly draining [*Borovsky et al.*, 1998a; *Borovsky and Steinberg*, 2006; *Borovsky and Denton*, 2008]. During recurrent high-speed-stream-driven storms the number density of the outer electron radiation belt at geosynchronous orbit also goes through an episodic cycle [*Borovsky et al.*, 1998a].

[3] Prior to most high-speed-stream-driven storms, intervals of unusually calm geomagnetic activity occur [*Borovsky and Steinberg*, 2005, 2006]. The working definition of a calm is a period where Kp dips below 1 and remains below 1.5 for at least 6 h. As explained by *Borovsky and Steinberg* [2006], these "calms before the storms" are caused by a Russell-McPherron effect acting on the Parker spiral magnetic field ahead of the sector reversal in the CIR (corotating interaction region): When it is Russell-McPherron favorable to have a storm after the CIR it is therefore Russell-McPherron favorable to have a calm before the CIR. This tendency for calms to occur before high-speed-stream-driven storms is demonstrated in Figure 1 (top), where the superposed average of the Kp index is plotted for 124 high-speed-stream-driven storms, where the zero epoch is the onset of storm levels of convection. The plot begins 20 days prior to storm onset. As can be seen, for the first 15 days of the plot the superposed average of the Kp index maintains at about 2.3 (gray dashed curve). Then about 5 days before storm onset the superposed average begins a systematic decrease. This average is decreasing because of the tendency of calms to occur before storms and the individual calms have various durations [cf. *Borovsky and Steinberg*, 2006]. During these calms before the storms [see also *Clilverd et al.*, 1993; *Borovsky et al.*, 1998a], the outer plasmasphere builds up out to large radii in the dipolar portions of the magnetosphere [*Denton and Borovsky*, 2008]. This buildup of cold-plasma density prior to storm onset can be seen in Figure 1 (bottom); the buildup begins about 5 days prior to storm onset in the superposed average of the measured cold-plasma density at geosynchronous orbit. It is anticipated that when the outer plasmasphere is present,

[1]Los Alamos National Laboratory, Los Alamos, New Mexico, USA.
[2]Department of Communication Systems, Lancaster University, Lancaster, UK.
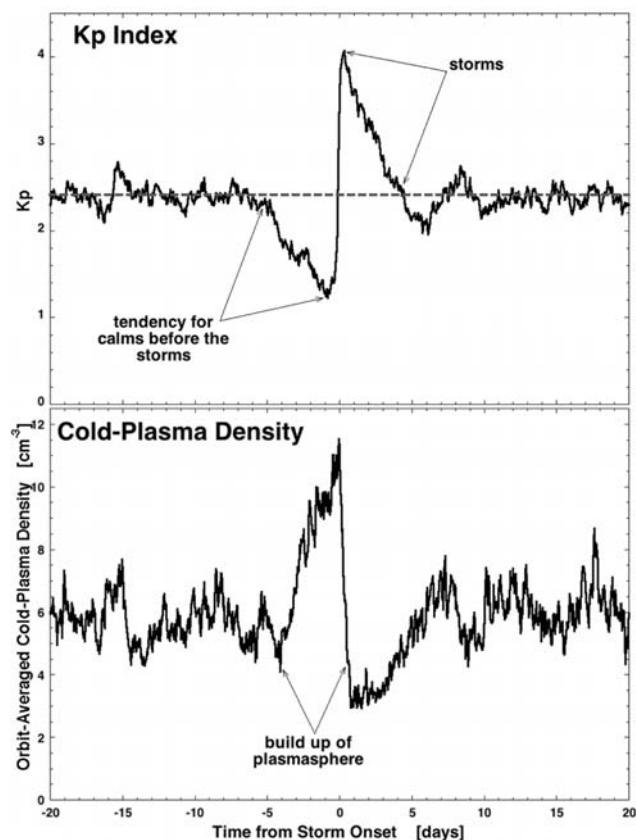
Figure 1. For 124 high-speed-stream-driven storms, (top) the superposed average of the Kp index and (bottom) the superposed average of the local-time-averaged cold-plasma density are plotted for 20 days prior to storm onset to 20 days after storm onset. The cold-plasma density is measured at geosynchronous orbit by the multisatellite MPA plasma detectors.

plasma waves that reside in the plasmasphere can pitch angle diffuse radiation belt electrons into the atmospheric loss cone [e.g., *Smith et al.*, 1974; *Kelley et al.*, 1975; *Albert*, 2004; *Summers et al.*, 2004; *Shprits and Thorne*, 2004], wherein the electrons are lost from the magnetosphere. Indeed, the number density of the outer radiation belt decreases with time in the days prior to high-speed-stream-driven storm onset [e.g., *Borovsky et al.*, 1998a, Figure 13; *Denton et al.*, 2009, Figure 7]. Other loss mechanisms, such as outward radial diffusion [e.g., *Brautigam and Albert*, 2000; *Shprits et al.*, 2006], magnetopause shadowing [e.g., *West et al.*, 1972; *Li et al.*, 1997; *Desorgher et al.*, 2000; *Bortnik et al.*, 2006a], and the Dst effect [e.g., *Dessler and Karplus*, 1961; *Kim and Chan*, 1997], should be reduced in importance during these geomagnetically calm intervals.

[4] Unlike high-speed-stream-driven storms wherein calms tend to occur prior to storm onset, calms do not tend to occur prior to coronal-mass-ejecta-driven storms [*Borovsky and Denton*, 2006]. In general, magnetic-cloud-driven (CME-driven) geomagnetic storms do not show a substantial loss of radiation belt electrons before the storm [cf. *Denton et al.*, 2009, Figure 8].

[5] Preliminary measurements of d(log(n))/dt from one spacecraft in 1993 and 1994 showed that the loss rates of

outer radiation belt electrons are higher during days when the outer plasmasphere is present than times when the outer plasmasphere is not seen [*Borovsky and Steinberg*, 2006]. These preliminary measurements yielded a loss rate for the radiation belt number density with an exponential e-folding time of 2.6 days in the presence of the plasmasphere. In that *Borovsky and Steinberg* [2006] study, this electron loss rate was overestimated owing to the inclusion of some radiation belt dropouts in the measurements.

[6] Recently, *Meredith et al.* [2006] measured the relativistic-electron flux decay rates for the outer electron radiation belt in the region $3.0 < L < 5.0$ during geomagnetically quiet periods: e-folding times for the fluxes of 1.5 to 6.5 days were obtained. These flux decay rates were similar to rates obtained from prior investigations in the $2.0 < L < 5.0$ region of the magnetosphere [e.g., *Lyons et al.*, 1972; *West et al.*, 1981; *Seki et al.*, 2005].

[7] Flux decay rates have also been measured for electrons in the inner radiation belt [e.g., *Pfitzer and Winckler*, 1968; *Tsurutani et al.*, 1975; *Selesnick et al.*, 2003; *Selesnick*, 2006; *Baker et al.*, 2007].

[8] In this report, the loss rates of electrons from the outer electron radiation belt at geosynchronous orbit will be measured using data superposition of 124 high-speed-stream-driven storms. The temporal changes in the number density of the outer electron radiation belt will be compared for storms with calms beforehand and storms without calms beforehand.

[9] This manuscript is organized as follows. In section 2 the spacecraft measurements and data analysis techniques utilized are discussed. In section 3 the measurements of the electron loss rates before storms are presented. In section 4 those loss rate measurements are used to calculate the fluxes of electrons into the upper atmosphere before geomagnetic storms. Section 5 contains discussions about the mechanisms leading to the electron loss, about the fluxes of electrons into the atmosphere, and about relativistic-electron dropouts at storm onset. Section 6 contains a summary of findings.

2. Density-Temperature Description of Outer Electron Radiation Belt

[10] Measurements of the number density n and the temperature T of the outer electron radiation belt at geosynchronous orbit are obtained as follows. The omnidirectional fluxes of energetic electrons are measured every 10 s by the Synchronous Orbit Particle Analyzer (SOPA) [*Belian et al.*, 1992; *Cayton and Belian*, 2007] onboard 7 satellites in geosynchronous orbit (6.6 R_E). The electrons are measured in the energy range ∼30 keV to >2 MeV. Relativistic bi-Maxwellian fits to the measured electrons fluxes are made every 10 s [cf. *Cayton et al.*, 1989; *Cayton and Belian*, 2007]. The bi-Maxwellian fitting describes two populations of electrons: a "soft" population of electrons with a temperature of ∼30 keV and a "hard" population of electrons with a temperature of ∼150 keV. The "soft" population is the suprathermal tail of the electron plasma sheet, which is strongly modulated at geosynchronous orbit by the occurrence of substorms [*Lezniak et al.*, 1968; *Birn et al.*, 1998]. The hard component is the outer electron radiation belt [*Cayton et al.*, 1989; *Belian et al.*, 1996].
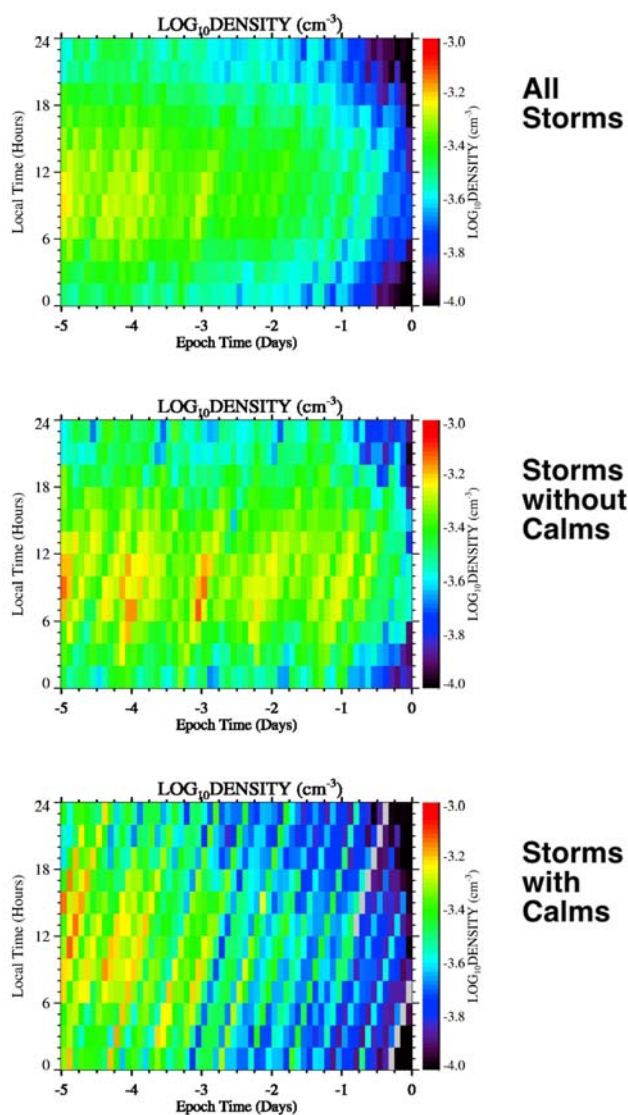
Figure 2. The base-10 logarithm of the number density of the outer electron radiation belt at geosynchronous orbit is plotted as functions of time (horizontal) and local time (vertical) for data superpositions triggered on storm onset. (top) The superposition is from 124 high-speed-stream-driven storms. (middle) The superposition is from a subset of 41 high-speed-stream-driven storms without calms beforehand. (bottom) The superposition is from a subset of 24 high-speed-stream-driven storms with calms beforehand.

[11] From the 10-s-resolution density and temperature measurements, median values of the density and temperature are calculated for every 30 min of measurement [cf. *Denton et al.*, 2009]. Taking only the median values reduces the influence of outliers when the fits are noisy.

[12] Changes in the number density n of the outer electron radiation belt are taken to be an indicator of the loss and gain of electrons from the magnetosphere and changes in the temperature T of the outer electron radiation belt are taken to be an indicator of the heating and cooling of the radiation belt electron population [cf. *Denton et al.*, 2009; J. E. Borovsky and M. H. Denton, Examining the

specific entropy (density of adiabatic invariants) of the outer electron radiation belt, submitted to *Journal of Geophysical Research*, 2009].

[13] To measure the loss rates of electrons from the outer radiation belt before storms, superposed data analysis for high-speed-stream-driven storms will be utilized. The t = 0 trigger for the data superposition will be the onset of storm levels of convection in the magnetosphere (storm onset). Relativistic-electron dropouts occur at about the time of storm onset [*Borovsky and Denton*, 2009], so with the superposed-epoch technique relativistic-electron dropouts can be clearly excluded from the measurements of electron loss rate. This will provide estimates of the electron loss rates prior to storms that are superior to the measurements made by *Borovsky and Steinberg* [2006]. The superposed-epoch analysis techniques follow the methodology of *Denton et al.* [2006].

[14] The superposed-epoch data analysis is performed on 124 high-speed-stream-driven storms that occurred between 1993 and 2006. The 124 events were collected by identifying corotating interaction regions (CIRs) in the solar wind (e.g., east/west flow deflections followed by sustained elevated wind speed) and then requiring a sustained level of high Kp (a storm) following the passage of the CIR [*Denton and Borovsky*, 2008, 2009; *Borovsky and Denton*, 2008, 2009]. If the storm in the Kp index did not repeat with a 27-day period, then the storm event was not included in the collection.

3. Density Loss During Calms Before Storms

[15] In each of the three plots of Figure 2, the base-10 logarithm of the number density n of the outer electron radiation belt is plotted in color as a function of time (horizontal axis) and local time (vertical axis). Figure 2 (top) is from a superposition of data from 124 high-speed-stream-driven storms, Figure 2 (middle) is from a superposition of data from a subset of 41 high-speed-stream-driven storms that definitely did not have calms beforehand, and Figure 2 (bottom) is from a superposition of a subset of 24 storms that clearly had well-defined calms beforehand. (59 storms wee note definitely in one category or the other.) In all three plots of Figure 2 time t = 0 is chosen to be the onset of storm levels of magnetospheric convection. Specifically, storm onset is detected by a strong rise in the Kp index [cf. *Elphic et al.*, 1999; *Thomsen*, 2004], with the final onset time calculated to ~30 min time resolution using changes in the MBI (Midnight Boundary Index) [*Madden and Gussenhoven*, 1990] to determine the time at which convection is equivalent to convection at a Kp value of 4^+. In Figure 2 (top) it is seen that the number density of the outer electron radiation belt decreases with time before high-speed-stream-driven storms. As can be seen by comparing Figure 2 (middle) and Figure 2 (bottom), for the storms with calms beforehand (Figure 2, bottom) the number density of the outer electron radiation belt at geosynchronous orbit decreases steadily with time in the days before the storm, whereas for the storms without calms (Figure 2, middle) the number density does not decrease as strongly prior to the storm onset. Note in Figure 2 (bottom) for the storms with calms that the number density decreases with time at all local times.
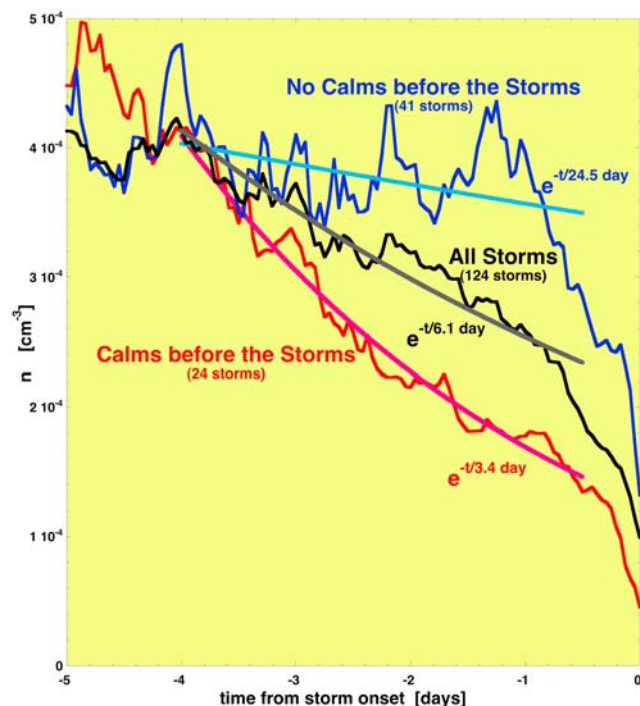
Figure 3. The local-time-averaged logarithm of the number density of the outer electron radiation belt at geosynchronous orbit is plotted as a function of time for data superpositions triggered on storm onset. The black curve is for 124 high-speed-stream-driven storms, the blue curve is for a subset of 41 storms without calms beforehand, and the red curve is for a subset of 24 storms with cams beforehand. Exponential fits to the data in the time range $t = -4$ days to $t = -0.5$ day are shown as the smooth curves.

[16] In Figure 3 the local-time-averaged logarithm of the number density n of the outer electron radiation belt at geosynchronous orbit is plotted as a function of time before the onset of high-speed-stream-driven storms. The three curves are for all 124 storms (black curve), storms without calms (blue curve), and storms with calms (red curve). The three curves represent the vertical integrals of the data in the three plots of Figure 2. In the time range from 4 days to 1/2 day before the storm onset, all three curves are fit with exponential functions (smooth curves in Figure 3) and the parameters of the fits are indicated. For the superposition of all high-speed-stream-driven storms (black curve), there is a distinctive decay of the number density n of the outer electron radiation belt in the days before storm onset: the exponential fit has a density e-folding time of 6.1 days. Note in Figure 3 the drastic difference in the number density decay rates between the storms with calms (red) and the storms without calms (blue). For storms with calms beforehand, the number density of the outer electron radiation belt at geosynchronous orbit begins to decay about 4 days prior to storm onset: the logarithmic average of the number density decreases from $\sim 4 \times 10^{-4}$ cm^{-3} to $\sim 1 \times 10^{-4}$ cm^{-3} in a few days. For storms with calms the exponential fit to the number density is of the form

$$n = 1.26 \times 10^{-4} \exp(-t/3.4 \text{ day}) \text{cm}^{-3} \qquad (1)$$

valid for $t = -4$ days to $t = -0.5$ day, an exponential decay with a 3.4-day e-folding time. For the storms without calms the exponential fit of the number density before the storm is $3.43 \times 10^{-4} \exp(-t/24.4 \text{ day})$ cm^{-3} valid for $t = -4$ days to $t = -0.5$ day, an exponential decay with a 24.4-day e-folding time. The decay rate is much stronger before the onset of storms with calms beforehand than it is before the onset of storms without calms beforehand.

[17] In Figure 4 the local time dependence of the temporal decay of the number density of the outer electron radiation belt at geosynchronous orbit is examined. In Figure 4 (left) and Figure 4 (right), exponential fits to the number density in the time range $t = -4$ days to $t = -0.5$ day (before storm onset) are plotted: The fits are to measurements taken at local noon (blue curves), local dawn (green curves), local dusk (red curves), and local midnight (black curves). The fits in Figure 4 (left) are for superpositions of data from 24 storms with calms beforehand and the fits in Figure 4 (right) are from 41 storms without calms beforehand. The functional forms of the fitted exponentials are indicated near each curve. As can be seen in Figure 4 (left), during calms the decay of the number density occurs at all local times with essentially the same decay rate (the same e-folding time).

[18] In Figure 5 several quantities describing the outer electron radiation belt at geosynchronous orbit are plotted as functions of time before high-speed-stream-driven storms. Figures 5a, 5c, 5e, and 5g pertain to storms with calms beforehand, and Figures 5b, 5d, 5f, and 5h pertain to storms without calms beforehand. In Figures 5a and 5b the number density n of the outer electron radiation belt is plotted, in Figures 5c and 5d the temperature T of the outer electron radiation belt is plotted, in Figures 5e and 5f the pressure $P = nk_BT$ of the outer electron radiation belt is plotted, and in Figures 5g and 5h the specific entropy $S = T/n^{2/3}$ of the outer electron radiation belt is plotted. Also plotted in gray Figures 5g and 5h is the relativistically corrected specific entropy $S_{rel} = T/n^{2/3} (1 + T/2mc^2)$ (cf. Borovsky and Denton, submitted manuscript, 2009). Time $t = 0$ is the onset of storm levels of magnetospheric convection. Exponential fits to the various curves are shown in gray in Figure 5 and the fit parameters are indicated in Figures 5a–5h and in Table 1. As can be seen in Figures 5c and 5d, the temperature of the outer electron radiation belt at geosynchronous orbit is nearly constant with time as the number density does or does not decay. The decay of the number density n for the storms with calms beforehand (Figures 5a, 5c, 5e, and 5g) leads to a temporal decay of the energy density (pressure P) of the outer electron radiation belt before the storm (Figure 5e): this temporal decay is approximately exponential with time (see fit). The specific entropy S has been shown to be a useful one-parameter description of the evolution of the outer electron radiation belts during all types of geomagnetic storms (Borovsky and Denton, submitted manuscript, 2009). The temporal decrease in the number density at constant temperature produces an increase in the specific entropy S (Figure 5g) of the outer electron radiation belt: this temporal increase is approximately exponential with time (see fits). The entropy changes throughout the phases of high-speed-stream-driven storms are discussed in greater detail by Borovsky and Denton (submitted manuscript, 2009). For the storms without the calms (Figures 5b,
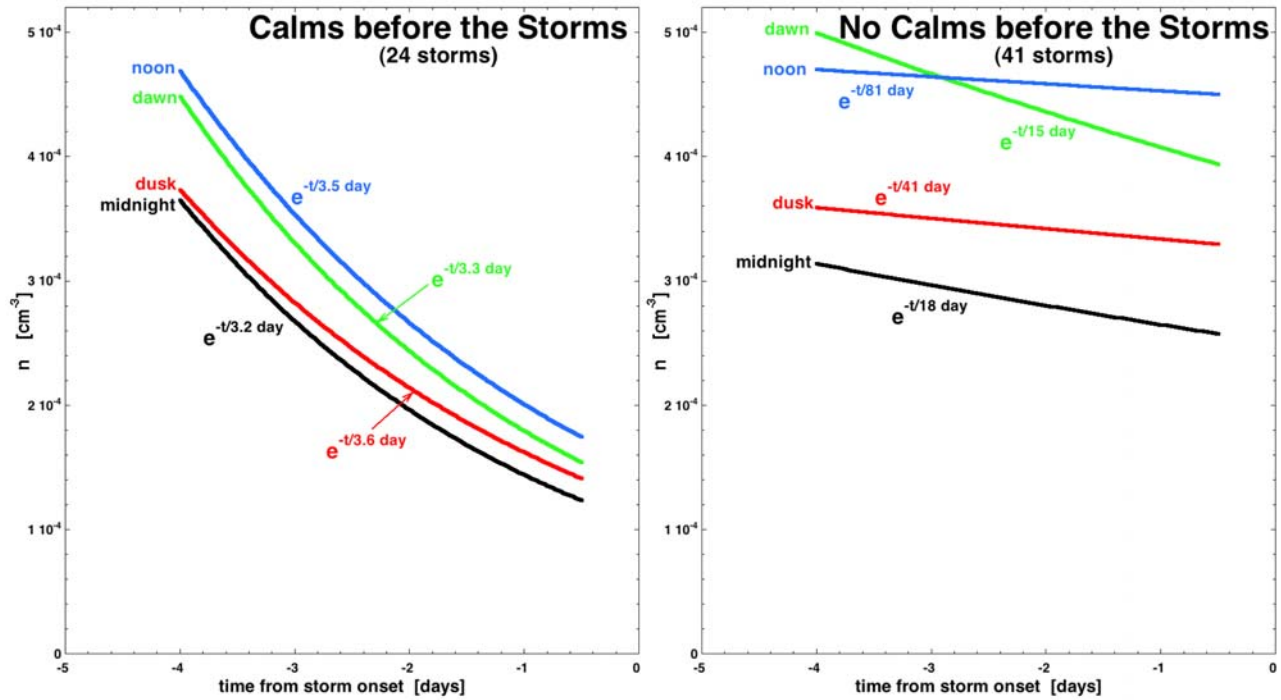
Figure 4. (left) For 24 storms with calms beforehand and (right) for 41 storms without calms beforehand, exponential fits to the superposed data are shown. The blue curve is for a 3-h-wide local time band around local noon, the green curve is for a 3-h-wide band around local dawn, the red curve is for a 3-h-wide band around local dusk, and the black curve is for a 3-h-wide band around local midnight.

5d, 5f, and 5h), the strong decrease of the pressure does not occur nor does the strong increase in the specific entropy occur.

[19] In Table 1 the fit parameters from Figure 5 for the number density n, temperature T, pressure P, specific entropy S, and relativistically corrected specific entropy S_{rel} are collected for storms with calms (Figures 5a, 5c, 5e, and 5g) and for storms without calms (Figures 5b, 5d, 5f, and 5h).

4. Electron Flux to the Atmosphere

[20] The electron flux from the outer electron radiation belt into the atmosphere is calculated as follows. The total number of electrons N in a flux tube of volume V is $N = nV$, where n is the number density of electrons in the flux tube. Taking the time derivative of this expression, the rate of change of the total number of electrons in the flux tube is given by

$$dN/dt = V\,dn/dt, \qquad (2)$$

where dn/dt is the rate of change of the number density n in the magnetosphere. Assuming that pitch angle scattering into the atmosphere is the only avenue for loss from the flux tube, the loss rate dN/dt of electrons from the flux tube is given by the flux of electrons F_{atm} into the atmosphere times the cross-sectional area A_{atm} of the flux tube in the atmosphere times 2 for two atmospheres (northern and southern):

$$dN/dt = 2F_{atm}A_{atm}. \qquad (3)$$

Equating expressions (2) and (3) yields

$$F_{atm} = (V/2A_{atm})dn/dt, \qquad (4)$$

where V/A_{atm} is the ratio of the volume of a flux tube to its cross-sectional area in the atmosphere and dn/dt is the rate of decay of the number density in the magnetosphere. By conservation of magnetic flux in the flux tube at the atmosphere and at the equator $B_{atm}A_{atm} = B_{eq}A_{eq}$, the area of the flux tube in the atmosphere A_{atm} can be expressed in terms of the area at the equator A_{eq} as

$$A_{atm} = A_{eq}(B_{eq}/B_{atm}), \qquad (5)$$

where B_{eq} and B_{atm} are the magnetic field strengths in the flux tube at the equator and at the atmosphere. With expression (5) for A_{atm}, expression (4) becomes

$$F_{atm} = (1/2)(V/A_{eq})(B_{atm}/B_{eq})dn/dt. \qquad (6)$$

At geosynchronous orbit (6.6 R_E), $V/A_{eq} = 7.6 \times 10^9$ cm (obtained by integrating a dipole field from one atmosphere to the other atmosphere [cf. *Borovsky et al.*, 1998b, Figure 4]), $B_{atm} = 0.56$ gauss [e.g., *Knecht and Schuman*, 1985], and $B_{eq} = 96$ nT (the median value as measured by the GOES 10 satellite in 2000–2003). The time derivative of expression (1) for n yields $dn/dt = 4.29 \times 10^{-10} \exp(-t/3.4 \text{ day})$ cm^{-3}s^{-1} valid for $t = -4$ days to $t = -0.5$ day. Using these values, expression (6) becomes

$$F_{atm} = 950\,e^{-t/3.4\,\text{day}}\text{cm}^{-2}\text{s}^{-1}. \qquad (7)$$
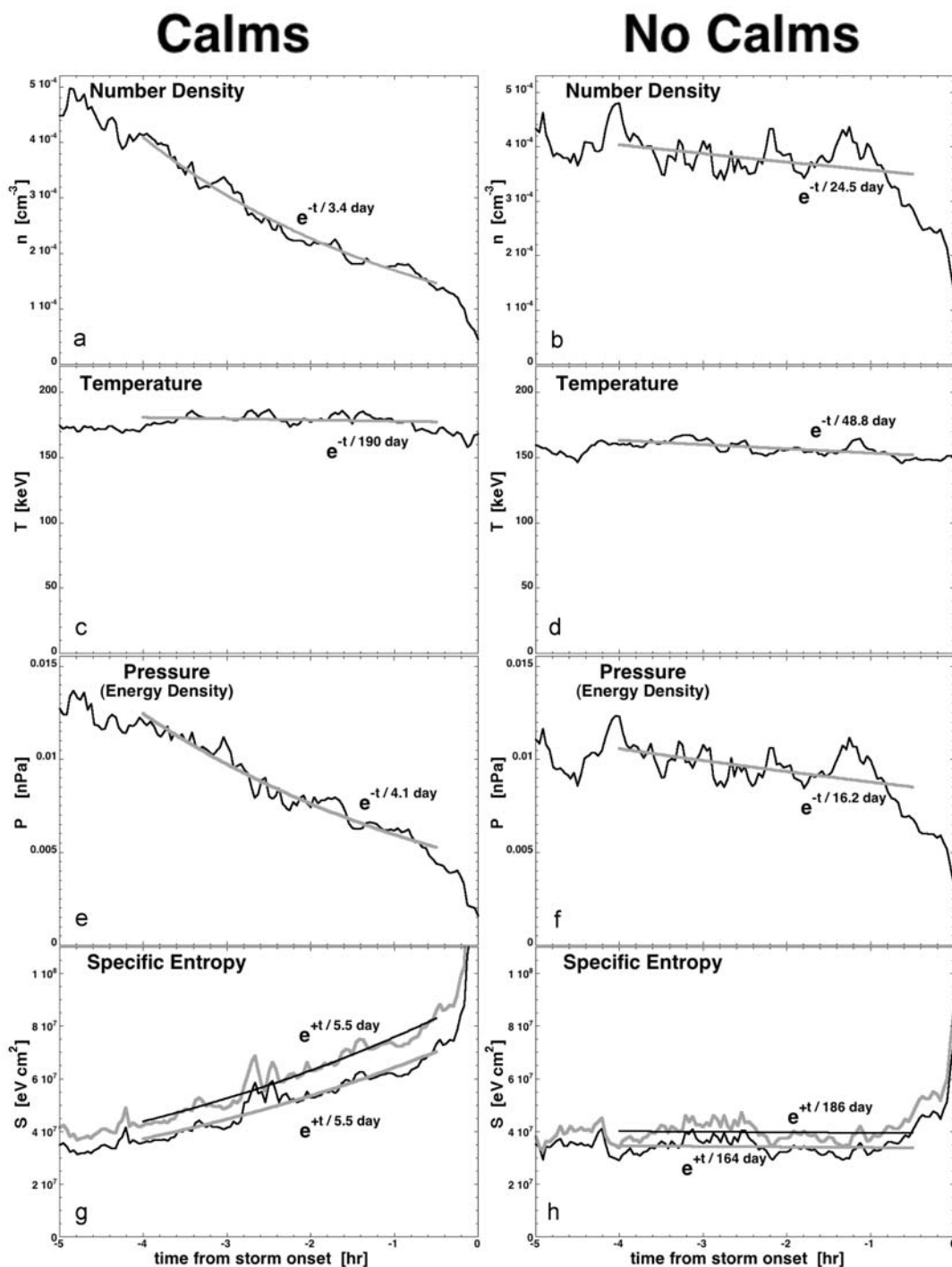
Calms

No Calms

Figure 5. (a, c, e, g) For a superposition of data from 24 high-speed-stream-driven storms with calms beforehand and (b, d, f, h) for a superposition of data from 41 high-speed-stream-driven storms without calms beforehand, the number density (Figures 5a and 5b), temperature (Figures 5c and 5d), pressure (Figures 5e and 5f), and specific entropy (Figures 5g and 5h) are plotted. The time t = 0 is the onset of storm convection. In Figures 5g and 5h, the gray curves are the relativistic version of the specific entropy.

At peak (t = −4 days) the electron flux into the atmosphere is $F_{atm} = 3080$ cm^{-2}s^{-1}.

[21] Note that if the precipitation rate of radiation belt electrons is not symmetric with local time [e.g., *Selesnick et al.*, 2003; *Clilverd et al.*, 2007; *Jordanova et al.*, 2008], then the fluxes to the atmosphere will be larger than expression (7) at some local times and lower than expression (7) at other local times.

[22] In the magnetosphere the thermal flux of electrons in the outer radiation belt is $F_{mag} \approx n v_{Te}$ where v_{Te} is the thermal velocity of the radiation belt electrons. At t = −4 days, the number density of the outer electron radiation belt is $n \approx 4 \times 10^{-4}$ cm^{-3} and the temperature is T =

Table 1. Exponential Fits for the Range −4 Days to −0.5 Day Before the Onset of High-Speed-Stream-Driven Storms

	Storms With Calms	Storm Without Calms
Number density n (cm^{-3})	$1.26 \times 10^{-4} \, e^{-t/3.40 \, \text{day}}$	$3.43 \times 10^{-4} \, e^{-t/24.5 \, \text{day}}$
Temperature T (keV)	$177 \, e^{-t/189.8 \, \text{day}}$	$150.4 \, e^{-t/48.8 \, \text{day}}$
Pressure P (nPa)	$4.66 \times 10^{-3} \, e^{-t/4.07 \, \text{day}}$	$8.82 \times 10^{-3} \, e^{-t/16.2 \, \text{day}}$
Specific entropy S (eV cm^2)	$7.71 \times 10^7 \, e^{+t/5.50 \, \text{day}}$	$3.37 \times 10^7 \, e^{+t/164.1 \, \text{day}}$
Relativistic specific entropy S_{rel} (eV cm^2)	$9.11 \times 10^7 \, e^{+t/5.47 \, \text{day}}$	$3.93 \times 10^7 \, e^{+t/185.6 \, \text{day}}$

170 keV (see Figure 5), which gives $v_{Te} \approx 1.6 \times 10^{10}$ cm/s. These values give $F_{mag} \approx 6.5 \times 10^6$ cm^{-2}s^{-1} at peak. Comparing this value 6.5×10^6 for the thermal flux in the magnetosphere to the value 3080 of the flux into the atmosphere at t = −4 days finds

$$F_{atm}/F_{mag} \approx 1/2100. \tag{8}$$

If strong diffusion of the radiation belt electrons were operating, the ratio in expression (8) would have a value on the order of unity. Since the ratio is $\sim10^{-3}$, the diffusion of electrons into the loss cone is ~3 orders of magnitude weaker than strong diffusion.

[23] Realizing that the particle pressure is the thermal energy density, the energy flux into the atmosphere from the outer electron radiation belt can be calculated from the decreasing pressure in the magnetosphere as follows. The total thermal energy content E of a flux tube of volume V is E = PV. Taking the time derivative of this, the loss rate of thermal energy dE/dt is hence

$$dE/dt = V \, dP/dt. \tag{9}$$

The loss rate of thermal energy from the flux tube into the atmosphere is

$$dE/dt = F_E 2A_{atm}, \tag{10}$$

where F_E is the thermal energy flux into the atmosphere and A_{atm} is the area of the flux tube in the atmosphere. Equating expressions (9) and (10) yields

$$F_E = (V/2A_{atm})dP/dt. \tag{11}$$

Again using expression (5) for A_{atm}, this becomes

$$F_E = (1/2)(V/A_{eq})(B_{atm}/B_{eq})dP/dt. \tag{12}$$

The temporal profile of the pressure of the outer electron radiation belt at geosynchronous orbit before a storm with a calm is of the form (see Figure 5 and see Table 1) P = 4.66×10^{-3} exp(−t/4.1 day) nPa, so the time derivative of the pressure is of the form dP/dt = 1.33×10^{-16} exp(−t/4.1 day) erg cm^{-2} s^{-1} (where 1 nPa = 10^8 erg cm^{-3} was used). Using this value of dP/dt along with $V/A_{eq} = 7.6 \times 10^9$ cm, $B_{eq} =$ 96 nT, and $B_{atm} = 0.56$ gauss, the energy flux into the atmosphere from the outer electron radiation belt at geosynchronous orbit is $F_E = 2.94 \times 10^{-4}$ exp(−t/4.1 day) erg cm^{-2} s^{-1} before the storm. At its strongest (time t = −4 days), this energy flux is $F_E = 7.8 \times 10^{-4}$ erg cm^{-2} s^{-1}. This energy flux is subvisual, with a flux of about 1 erg cm^{-2} s^{-1} being required to produce visual airglow [Seaton, 1954; Dalgarno et al., 1965]. (Note that since the radiation belt electrons deposit their energy deeper in the atmosphere than typical aurora, collisional quenching of the 5577-Å emission will require an energy flux of greater than 1 erg cm^{-2} s^{-1} to produce visible emission.)

5. Discussion

[24] The discussion in this section focuses on three topics: (1) the interpretation of the observed decay in the number density of the outer electron radiation belt at geosynchronous orbit, (2) the potential consequences of the fluxes of radiation belt electrons into the atmosphere, and (3) the relativistic-electron dropouts at the onset of high-speed-stream-driven storms which follow in time the slow decay during calms.

5.1. Interpretation of Loss: Waves in the Plasmasphere

[25] The greatly enhanced loss of electrons from the outer radiation belt during calms before storms is believed to be caused by the buildup of the outer plasmasphere during the calms [Borovsky and Steinberg, 2005, 2006], leading to pitch angle scattering of the radiation belt electrons by plasma waves in the plasmasphere [Smith et al., 1974; Kelley et al., 1975; Albert, 2004; Summers et al., 2004; Shprits and Thorne, 2004]. During these calms other loss mechanisms such as the Dst effect, radial diffusion, and magnetopause shadowing should be reduced. The specific plasma wave candidates to pitch angle scatter the electrons of the outer radiation belt are (whistler mode) plasmaspheric hiss [cf. Lyons et al., 1972; Meredith et al., 2006; Lam et al., 2007], lightning-generated whistlers [cf. Voss et al., 1998; Lauben et al., 2001; Rodger et al., 2003; Bortnik et al., 2006b], and electromagnetic ion cyclotron waves [cf. Summers and Thorne, 2003; Albert, 2003].

[26] The differences in the rates of decay between periods of calms versus periods that are not calm has been interpreted as the result of their being an outer plasmasphere versus their being no outer plasmasphere. However, calms can occur without the outer plasmasphere building up, and conversely there can be a built-up outer plasmasphere in the absence of calm. Indeed, an inspection the 24 storms with calms beforehand finds several cases without outer plasmaspheres and an inspection of the 41 storms without calms beforehand finds several such cases with built-up outer plasmaspheres.

[27] To clarify the role that the outer plasmasphere plays in the decay of the electron-radiation-belt density, a set of high-speed-stream-driven storms that have built-up outer plasmaspheres before onset is compared with a set of high-speed-stream-driven storms without built-up outer plasmaspheres beforehand. The temporal profile of the superposed temperature of the outer electron radiation belt is plotted in Figure 6 (top) and the temporal profile of the superposed number density of the outer electron radiation belt is plotted
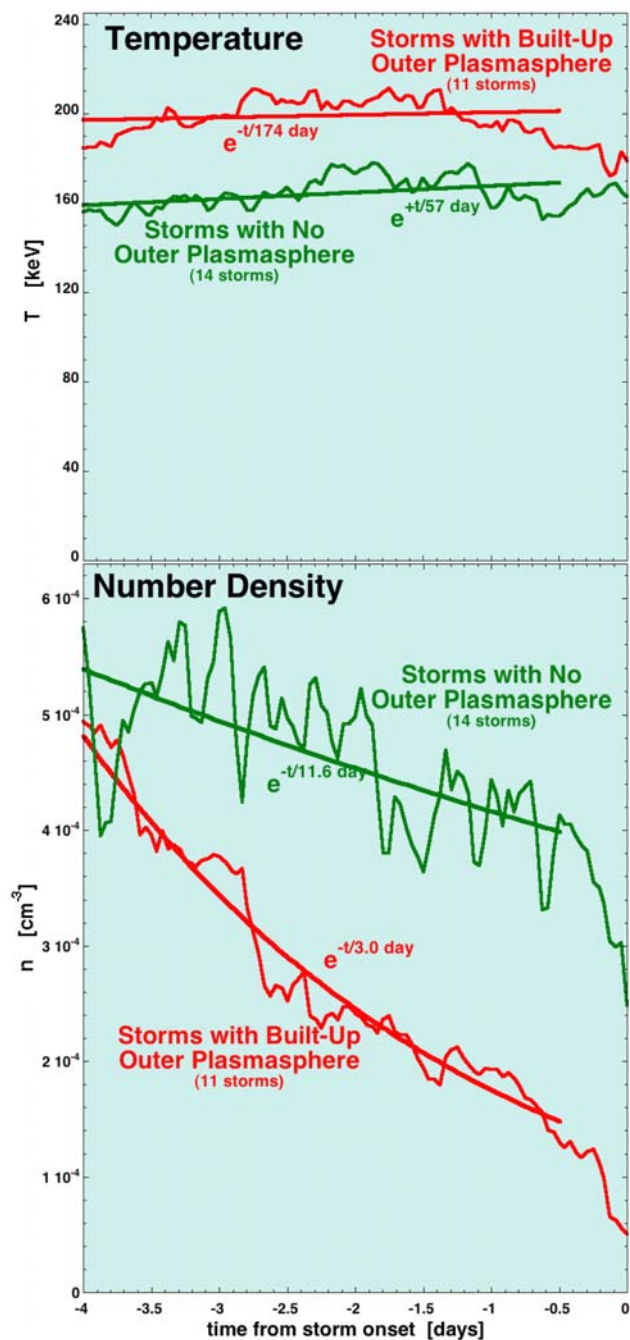
Figure 6. For data superpositions of high-speed-stream-driven storms, the (top) local-time-averaged temperature and (bottom) number density of the outer electron radiation belt at geosynchronous orbit are plotted as a function of time. Time t = 0 is the storm onset. The green curves are for 14 storms without calms beforehand and without built-up outer plasmaspheres. The red curves are for 11 storms with calms beforehand and with built-up outer plasmaspheres. The smooth curves are exponential fits of the data between t = −4 days and t = −0.5 day.

in Figure 6 (bottom); the green curves are for 14 storms with no calms beforehand and with an absence of outer plasmaspheric plasma and the red curves are for 11 storms with calms beforehand that also have built-up outer plasma-

spheres at geosynchronous orbit for 2 or more days prior to storm onset. The absence or presence of a built-up outer plasmasphere is determined by an examination of the cold-plasma measurements made by the Magnetospheric Plasma Analyzer (MPA) [*Bame et al.*, 1993] onboard the Los Alamos geosynchronous satellites; at geosynchronous orbit the outer plasmasphere is present when dense cold plasma is measured at most local times [e.g., *Sojka and Wrenn*, 1985; *Lawrence et al.*, 1999; *Su et al.*, 2001] and the outer plasmasphere is absent when dense cold plasma is only seen for a few hours of local time in the dusk sector. (The cold plasma in the dusk sector is the duskside bulge of the plasmasphere extending beyond geosynchronous orbit [cf. *Chappell et al.*, 1970; *Higel and Lei*, 1984; *Moldwin et al.*, 1994]). The determination of where in local time dense cold plasma resides is made by a visual inspection of the MPA daily ion-energy color spectrograms from the multiple geosynchronous satellites; roughly, a cold-plasma number density of 10 cm^{-3} represents the presence of plasmaspheric material. As can be seen in Figure 6 (bottom), before storm onset the radiation belt electron density decays strongly in time for storms wherein there is a built up outer plasmasphere in comparison with storms wherein the outer plasmasphere is absent. For storms with confirmed outer plasmaspheres the exponential decay of the number density has an e-folding time of 3.0 days, compared to the 11.6-day e-folding time for storms without outer plasmaspheres. This 3.0-day decay (Figure 6) is slightly faster than the 3.4-day decay measured for storms with calms (Figures 3 and 5); some calms do not have built-up plasmaspheres. The 11.6-day decay (Figure 6) is faster than the 24.5-day decay measured for storms without calms (Figures 3 and 5); some intervals of no calm do have built-up plasmaspheres. The decay rates of Figure 6 are better measures of the decay rates when the outer plasmasphere is definitely present (decay rate = 3.0 days) and definitely absent (decay rate = 11.6 days). As noted at the beginning of section 5.1, the 3.0-day decay rate for storms with outer plasmaspheres present may be measurements of the decay of the electron radiation belt owing to whistler mode hiss and electromagnetic ion cyclotron waves in the outer plasmasphere. Conversely, the 11.6-day decay rate for storms without outer plasmaspheres present may be measurements of the decay of the electron radiation belt owing to whistler mode hiss and electromagnetic ion cyclotron waves in the duskside bulge of the plasmasphere [e.g., *Carpenter*, 1970; *Koons and Roeder*, 1990; *Bespalov et al.*, 1990; *Lorentzen et al.*, 2000; *Jordanova et al.*, 2003] and to whistler mode chorus waves outside the plasmapause [e.g., *Glauert and Horne*, 2005; *Thorne et al.*, 2005; *Shprits et al.*, 2007]. Note that whistler mode chorus is also anticipated to heat the electron radiation belt [cf. *Summers et al.*, 1998; *Meredith et al.*, 2002; *Horne and Thorne*, 2003; *Horne et al.*, 2005; *Bortnik and Thorne*, 2007] in addition to scattering its electrons into the loss cone: As can be seen by examining the green curve in Figure 6 (top), no significant change in the temperature of the outer electron radiation belt is seen as the number density decays in the absence of an outer plasmasphere.

[28] Note that ejecta-driven geomagnetic storms do not show a trend of decaying number density of the outer electron radiation belt at geosynchronous orbit in the days before storm onset (cf. Borovsky and Denton, submitted

manuscript, 2009, Figure 10). This may be because ejecta-driven storms do not tend to have calms occurring before storm onset [*Borovsky and Steinberg*, 2006; *Borovsky and Denton*, 2006] and hence they do not tend to have built-up outer plasmaspheres before the storms.

5.2.   Fluxes of Energetic Electrons Into the Atmosphere

[29]   In section 4 it was calculated that the electron fluxes from the outer electron radiation belt at geosynchronous orbit into the atmosphere are about $F_{atm} \approx 3080$ cm^{-2}s^{-1} at their highest during calms before high-speed-stream-driven storms if the precipitating fluxes are uniform in local time. (If the precipitating fluxes are not uniform in local time, the fluxes will be higher than 3080 cm^{-2}s^{-1}.) These fluxes into the atmosphere are about 1/2100 times as strong as thermal fluxes in the outer electron radiation belt in the magneto-sphere, indicating that the diffusion into the loss cone during calms is 3 orders of magnitude weaker than strong diffusion. In section 4 it was also calculated that the energy flux of these radiation belt electrons is on the order of $F_E \approx 7.8 \times 10^{-4}$ erg cm^{-2} s^{-1} (if it is uniform in local time). These 7.8×10^{-4} erg cm^{-2} s^{-1} fluxes are subvisual in terms of the production of airglow.

[30]   Even though the relativistic-electron fluxes to the atmosphere during calms before storms are subvisual, the precipitation of these electrons into the atmosphere should not be ignored [cf. *Thorne*, 1980; *Baker et al.*, 1993; *Lastovicka*, 1996; *Siskind*, 2002]. Precipitating electrons with energies of 150 keV and above deposit most of their energy at altitudes of about 75 km and lower [e.g., *Rees*, 1963, 1964]. The effects of energetic electrons on atmo-spheric chemistry [e.g., *Thorne*, 1997; *Callis et al.*, 1991, 1998; *Rozanov et al.*, 2005; *Randall et al.*, 2007], iono-spheric profiles [e.g., *Larsen et al.*, 1976; *Goldberg et al.*, 1984; *Frahm et al.*, 1997; *Rodger et al.*, 2007], atmospheric electricity [e.g., *Sheldon et al.*, 1988; *Tinsley et al.*, 2007], and climate [e.g., *Lastovicka*, 1996; *Kniveton and Tinsley*, 2004] are presently being considered. Calms before storms precondition the magnetosphere for the storms in several ways [cf. *Borovsky and Steinberg*, 2006; *Borovsky and Denton*, 2006]. This enhanced precipitation from the outer electron radiation belts during calms may provide an avenue for the solar wind upstream of CIRs to precondition the atmosphere and the ionosphere for the high-speed-stream-driven storms. Preconditioning aside, there may be impor-tant atmospheric and ionospheric effects in the days leading up to storms and we suggest that future research projects could discern such effects statistically by means of super-posed-epoch studies such as the studies of this report.

5.3.   Electron Fluxes Into the Atmosphere During Relativistic-Electron Dropouts

[31]   In comparison with the electron fluxes during calms before the storms, the electron fluxes from the outer radiation belt into the atmosphere during relativistic-elec-tron dropouts at storm onset are more than an order of magnitude more intense. In a relativistic-electron dropout the number density decreases by more than 1×10^{-4} cm^{-3} in about 6 h [*Borovsky and Denton*, 2009; Borovsky and Denton, submitted manuscript, 2009]. This gives a dn/dt value of dn/dt $\approx 5 \times 10^{-9}$ cm^{-3} s^{-1}, which is 3.5 times larger than the dn/dt $= 1.4 \times 10^{-9}$ cm^{-3} s^{-1} value for

calms. During relativistic-electron dropouts the loss of electrons probably does not occur at all local times, but rater it is confined to the plasmaspheric drainage plume in the afternoon sector. At geosynchronous orbit, plumes are about 4 h wide in local time at the onset of high-speed-stream-driven storms [*Borovsky and Denton*, 2008], which boosts the local flux by a factor of 24/4 = 6. With the 3.5 factor increase in dn/dt and the factor 6 increase for local time effects, the electron flux into the atmosphere is $F_{atm} \approx 2 \times 10^5$ cm^{-2} s^{-1}. For $n = 2 \times 10^{-4}$ cm^{-3} and T = 170 keV, the thermal flux in the outer electron radiation belt in the magnetosphere is $F_{mag} \approx 3.2 \times 10^6$ cm^{-2} s^{-1}. Comparing these two numbers finds $F_{atm}/F_{mag} \approx 1/16$. The pitch angle diffusion rate during relativistic-electron dropouts is about 1 order of magnitude weaker than strong diffusion. If the precipitation of electrons from the outer radiation belt maps to only a portion of the plasmaspheric drainage plume during relativistic-electron dropouts, then the flux to the atmosphere is higher and the diffusion may be strong diffusion.

[32]   During the relativistic-electron dropouts at storm onset, the energy flux into the atmosphere from the outer radiation belt is larger than the energy flux during calms before the storms. With dn/dt = 5×10^{-9} cm^{-3} s^{-1}, T = 170 keV, and a 5-h wide plume, the estimated energy flux into the atmosphere is $F_E \approx 0.9$ erg cm^{-2} s^{-1}, approxi-mately the 1 erg cm^{-2} s^{-1} to produce visible airglow.

6.   Summary

[33]   There is a slow decay of the number density n of the outer electron radiation belt at geosynchronous orbit during calms before high-speed-stream-driven storms. The decay starts about 4 days prior to storm onset. When there is no calm before the storm, the decay in the number density is very slight. No calm, no loss. The specific findings of this study are the following.

[34]   1. The decay of the number density is believed to be caused by electrons being pitch angle scattered into the atmospheric loss cone by plasma waves in the outer plasma-sphere, which grows during the calms.

[35]   2. When storms without outer plasmaspheres before-hand are compared with storms with outer plasmaspheres beforehand, a distinct difference in the decay rate of the number density of the outer electron radiation belt at geosynchronous orbit is observed. The e-folding lifetime of the number density is 3.0 days when the outer plasma-sphere is present and the lifetime is 11.6 days when the outer plasmasphere is absent.

[36]   3. The number density decay rate during the calms before the storms is fit as n = 1.26×10^{-4} e$^{-t/3.40 \text{ day}}$ cm^{-3} (valid for t = −4 days to t = −0.5 day), which has an exponential e-folding decay time of 3.4 days.

[37]   4. The rate of decay of the number density n of the outer electron radiation belt at geosynchronous orbit is similar at all local times.

[38]   5. During calms before storms, as the number density n steadily decays, the temperature T of the outer electron radiation belt at geosynchronous orbit stays approximately constant. The temperature remaining constant as the elec-trons precipitate to the atmosphere indicates that the pitch

angle scattering into the loss cone acts equally at all energies.

[39] 6. During calms before storms, as the number density of the outer electron radiation belt decreases the pressure P of the outer electron radiation belt decreases. If there is no calm, there is no decrease in the pressure of the outer electron radiation belt. This pressure is equal to the thermal energy density of the outer electron radiation belt.

[40] 7. During calms before storms, as the number density of the outer electron radiation belt decreases the specific entropy S of the outer electron radiation belt increases. If there is no calm, there is no increase in the specific entropy of the outer electron radiation belt.

[41] 8. The flux of outer radiation belt electrons into the atmosphere is 3 orders of magnitude less than the thermal flux of outer radiation belt electrons in the magnetosphere, indicating that the scattering into the loss cone is 3 orders of magnitude slower than strong diffusion.

[42] 9. The deposition of energy into the atmosphere by the precipitating outer radiation belt electrons at geosynchronous orbit during calms is too small to produce visible airglow.

[43] 10. Relativistic-electron dropouts at storm onset follow the decay of the outer electron radiation belt during calms before the storms. If there is a calm before the storm, the relativistic-electron dropout is deeper [*Borovsky and Denton*, 2009; Borovsky and Denton, submitted manuscript, 2009]. During relativistic-electron dropouts the local fluxes of electrons into the atmosphere are much higher (but briefer) than during calms before storms.

References

Albert, J. M. (2003), Evaluation of quasi-linear diffusion coefficients for EMIC waves in a multispecies plasma, *J. Geophys. Res.*, *108*(A6), 1249, doi:10.1029/2002JA009792.

Albert, J. M. (2004), Using quasi-linear diffusion to model acceleration and loss from wave-particle interactions, *Space Weather*, *2*, S09S03, doi:10.1029/2004SW000069.

Baker, D. N., R. A. Goldberg, F. A. Herrero, J. B. Blake, and L. B. Callis (1993), Satellite and rocket studies of relativistic electrons and their influence on the middle atmosphere, *J. Atmos. Terr. Phys.*, *55*, 1619, doi:10.1016/0021-9169(93)90167-W.

Baker, D. N., S. G. Kanekal, R. B. Horne, N. P. Meredith, and S. A. Glauert (2007), Low-altitude measurements of 2−6 MeV electron trapping lifetimes at $1.5 \leq L \leq 2.5$, *Geophys. Res. Lett.*, *34*, L20110, doi:10.1029/2007GL031007.

Bame, S. J., D. J. McComas, M. F. Thomsen, B. L. Barraclough, R. C. Elphic, J. P. Glore, J. T. Gosling, J. C. Chavez, E. P. Evans, and F. J. Wymer (1993), Magnetospheric plasma analyzer for spacecraft with constrained resources, *Rev. Sci. Instrum.*, *64*, 1026, doi:10.1063/1.1144173.

Belian, R. D., G. R. Gisler, T. Cayton, and R. Christensen (1992), High-Z energetic particles at geosynchronous orbit during the great solar proton event series of October 1989, *J. Geophys. Res.*, *97*, 16,897, doi:10.1029/92JA01139.

Belian, R. D., T. E. Cayton, R. A. Christiansen, J. C. Ingraham, M. M. Meier, G. D. Reeves, and A. J. Lazarus (1996), Relativistic electrons in the outer-zone: An 11 year cycle; Their relation to the solar wind, in *Workshop on the Earth's Trapped Particle Environment*, edited by G. D. Reeves, *AIP Conf. Proc.*, *383*, 13.

Bespalov, P. A., A. Grafe, A. G. Demekhov, and V. Y. Trakhtengerts (1990), Some aspects of the dynamics of the asymmetric ring current, *Geomagn. Aeron.*, *30*, 628.

Birn, J., M. F. Thomsen, J. E. Borovsky, G. D. Reeves, D. J. McComas, R. D. Belian, and M. Hesse (1998), Substorm electron injections: Geosynchronous observations and test particle simulations, *J. Geophys. Res.*, *103*, 9235, doi:10.1029/97JA02635.

Borovsky, J. E, and M. H. Denton (2006), The differences between CME-driven storms and CIR-driven storms, *J. Geophys. Res.*, *111*, A07S08, doi:10.1029/2005JA011447.

Borovsky, J. E., and M. H. Denton (2008), A statistical look at plasmaspheric drainage plumes, *J. Geophys. Res.*, *113*, A09221, doi:10.1029/2007JA012994.

Borovsky, J. E., and M. H. Denton (2009), Relativistic-electron dropouts and recovery: A superposed epoch study of the magnetosphere and the solar wind, *J. Geophys. Res.*, *114*, A02201, doi:10.1029/2008JA013128.

Borovsky, J. E., and J. T. Steinberg (2005), The calm before the storm in CIR/magnetosphere interactions, *Eos Trans. AGU*, *86*(52), Fall Meet. Suppl., Abstract SM54A-05.

Borovsky, J. E., and J. T. Steinberg (2006), The "calm before the storm" in CIR/magnetosphere interactions: Occurrence statistics, solar-wind statistics, and magnetospheric preconditioning, *J. Geophys. Res.*, *111*, A07S10, doi:10.1029/2005JA011397.

Borovsky, J. E., M. F. Thomsen, D. J. McComas, T. E. Cayton, and D. J. Knipp (1998a), Magnetospheric dynamics and mass flow during the November 1993 storm, *J. Geophys. Res.*, *103*, 26,373, doi:10.1029/97JA03051.

Borovsky, J. E., M. F. Thomsen, R. C. Elphic, T. E. Cayton, and D. J. McComas (1998b), The transport of plasma sheet material from the distant tail to geosynchronous orbit, *J. Geophys. Res.*, *103*, 20,297, doi:10.1029/97JA03144.

Bortnik, J., and R. M. Thorne (2007), The dual role of ELF/VLF chorus waves in the acceleration and precipitation of radiation belt electrons, *J. Atmos. Sol. Terr. Phys.*, *69*, 378, doi:10.1016/j.jastp.2006.05.030.

Bortnik, J., R. M. Thorne, T. P. O'Brien, J. C. Green, R. J. Strangeway, Y. Y. Shprits, and D. N. Baker (2006a), Observation of two distinct, rapid loss mechanisms during the 20 November 2003 radiation belt dropout event, *J. Geophys. Res.*, *111*, A12216, doi:10.1029/2006JA011802.

Bortnik, J., U. S. Inan, and T. F. Bell (2006b), Temporal signatures of radiation belt electron precipitation induced by lightning-generated MR whistler waves: 2. Global signatures, *J. Geophys. Res.*, *111*, A02205, doi:10.1029/2005JA011398.

Brautigam, D. H., and J. M. Albert (2000), Radial diffusion analysis of outer radiation belt electrons during the October 9, 1990, magnetic storm, *J. Geophys. Res.*, *105*, 291, doi:10.1029/1999JA900344.

Callis, L. B., D. N. Baker, J. B. Blake, J. D. Lambeth, R. E. Boughner, M. Natarajan, R. W. Klebesadel, and D. J. Gorney (1991), Precipitating relativistic electrons: Their long-term effect on stratospheric odd nitrogen levels, *J. Geophys. Res.*, *96*, 2939, doi:10.1029/90JD02184.

Callis, L. B., M. Natarajan, J. D. Lambeth, and D. N. Baker (1998), Solar-atmospheric coupling by electrons (SOLACE): 2. Calculated stratospheric effects of precipitating electrons, *J. Geophys. Res.*, *103*, 28,421, doi:10.1029/98JD02407.

Carpenter, D. L. (1970), Whistler evidence of the dynamic behavior of the duskside bulge in the plasmasphere, *J. Geophys. Res.*, *75*, 3837, doi:10.1029/JA075i019p03837.

Carpenter, D. L., B. L. Giles, C. R. Chappell, P. M. E. Decreau, R. R. Anderson, A. M. Persoon, A. J. Smith, Y. Corcuff, and P. Canu (1993), Plasmasphere dynamics in the duskside bulge region: A new look at an old topic, *J. Geophys. Res.*, *98*, 19,243, doi:10.1029/93JA00922.

Cayton, T. E., and R. D. Belian (2007), Numerical modeling of the synchronous orbit particle analyzer, *Los Alamos Natl. Lab. Rep. LA-14335*, Los Alamos, N. M., June.

Cayton, T. E., R. D. Belian, S. P. Gary, T. A. Fritz, and D. N. Baker (1989), Energetic electron components at geosynchronous orbit, *Geophys. Res. Lett.*, *16*, 147, doi:10.1029/GL016i002p00147.

Chappell, C. R., K. K. Harris, and G. W. Sharp (1970), The morphology of the bulge region of the plasmasphere, *J. Geophys. Res.*, *75*, 3848, doi:10.1029/JA075i019p03848.

Clilverd, M. A., T. D. G. Clark, A. J. Smith, and N. R. Thomson (1993), Observation of a decrease in mid-latitude whistler-mode signal occurrence prior to geomagnetic storms, *J. Atmos. Terr. Phys.*, *55*, 1479, doi:10.1016/0021-9169(93)90113-D.

Clilverd, M. A., N. P. Meredith, R. B. Horne, S. A. Glauert, R. R. Anderson, N. R. Thomson, F. W. Menk, and B. R. Sandel (2007), Longitudinal and seasonal variations in plasmaspheric electron density: Implications for electron precipitation, *J. Geophys. Res.*, *112*, A11210, doi:10.1029/2007JA012416.

Dalgarno, A., I. D. Latimer, and J. W. McConkey (1965), Corpuscular bombardment and N_2^+ radiation, *Planet. Space Sci.*, *13*, 1008, doi:10.1016/0032-0633(65)90160-1.

Denton, M. H., and J. E. Borovsky (2008), Superposed epoch analysis of high-speed-stream effects at geosynchronous orbit: Hot plasma, cold plasma, and the solar wind, *J. Geophys. Res.*, *113*, A07216, doi:10.1029/2007JA012998.

Denton, M. H., and J. E. Borovsky (2009), The superdense plasma sheet in the magnetosphere during high-speed-stream-driven storms: Plasma transport timescales, *J. Atmos. Sol. Terr. Phys.*, *71*, 1045–1058, doi:10.1016/j.jastp.2008.04.023.

Denton, M. H., J. E. Borovsky, R. M. Skoug, M. F. Thomsen, B. Lavraud, M. G. Henderson, R. L. McPherron, J. C. Zhang, and M. W. Liemohn (2006), Geomagnetic storms driven by ICME- and CIR-dominated solar wind, *J. Geophys. Res.*, *111*, A07S07, doi:10.1029/2005JA011436.

Denton, M. H., J. E. Borovsky, and T. E. Cayton (2009), A density-temperature description of the outer electron radiation belt during geomagnetic storms, *J. Geophys. Res.*, doi:10.1029/2009JA014183, in press.

Desorgher, L., E. Fluckiger, P. Buhler, and A. Zehnder (2000), Modelling of the outer electron belt flux dropout and losses during magnetic storm main phase, *Adv. Space Res.*, *26*, 167, doi:10.1016/S0273-1177(99)01044-3.

Dessler, A. J., and R. Karplus (1961), Some effects of diamagnetic ring currents on Van Allen radiation, *J. Geophys. Res.*, *66*, 2289, doi:10.1029/JZ066i008p02289.

Elphic, R. C., M. F. Thomsen, and J. E. Borovsky (1997), The fate of the outer plasmasphere, *Geophys. Res. Lett.*, *24*, 365, doi:10.1029/97GL00141.

Elphic, R. C., M. F. Thomsen, J. E. Borovsky, and D. E. McComas (1999), Inner edge of the electron plasma sheet: Empirical models of boundary location, *J. Geophys. Res.*, *104*, 22,679.

Frahm, R. A., J. D. Winningham, J. R. Sharber, R. Link, G. Crowley, E. E. Gaines, D. L. Chenette, B. J. Anderson, and T. A. Potemra (1997), The diffuse aurora: A significant source of ionization in the middle atmosphere, *J. Geophys. Res.*, *102*, 28,203, doi:10.1029/97JD02430.

Glauert, S. A., and R. B. Horne (2005), Calculation of pitch angle and energy diffusion coefficients with the PADIE code, *J. Geophys. Res.*, *110*, A04206, doi:10.1029/2004JA010851.

Goldberg, R. A., C. H. Jackman, J. R. Barcus, and F. Soras (1984), Nighttime auroral energy deposition in the middle atmosphere, *J. Geophys. Res.*, *89*, 5581, doi:10.1029/JA089iA07p05581.

Higel, B., and W. Lei (1984), Electron density and plasmapause characteristics at 6.6 R_E: A statistical study of GEOS 2 relaxation sounder data, *J. Geophys. Res.*, *89*, 1583, doi:10.1029/JA089iA03p01583.

Horne, R. B., and R. M. Thorne (2003), Relativistic electron acceleration and precipitation during resonant interactions with whistler-mode chorus, *Geophys. Res. Lett.*, *30*(10), 1527, doi:10.1029/2003GL016973.

Horne, R. B., R. M. Thorne, S. A. Glauert, J. M. Albert, N. P. Meredith, and R. R. Anderson (2005), Timescale for radiation belt electron acceleration by whistler mode chorus waves, *J. Geophys. Res.*, *110*, A03225, doi:10.1029/2004JA010811.

Jordanova, V. K., A. Boonsiriseth, R. M. Thorne, and Y. Dotan (2003), Ring current asymmetry from global simulations using a high-resolution electric field model, *J. Geophys. Res.*, *108*(A12), 1443, doi:10.1029/2003JA009993.

Jordanova, V. K., J. Albert, and Y. Miyoshi (2008), Relativistic electron precipitation by EMIC waves from self-consistent global simulations, *J. Geophys. Res.*, *113*, A00A10, doi:10.1029/2008JA013239.

Kelley, M. C., B. T. Tsurutani, and F. S. Mozer (1975), Properties of ELF electromagnetic waves in and above the Earth's ionosphere deduced from plasma wave experiments on the OVI-17 and Ogo 6 satellites, *J. Geophys. Res.*, *80*, 4603, doi:10.1029/JA080i034p04603.

Kim, H.-J., and A. A. Chan (1997), Fully adiabatic changes in storm time relativistic electron fluxes, *J. Geophys. Res.*, *102*, 22,107, doi:10.1029/97JA01814.

Knecht, D. J., and B. M. Schuman (1985), The geomagnetic field, in *Handbook of Geophysics and the Space Environment*, edited by A. S. Jursa, p. 4-1, Natl. Tech. Inf. Serv., Springfield, Va.

Kniveton, D. R., and B. A. Tinsley (2004), Daily changes in global cloud cover and Earth transits of the heliospheric current sheet, *J. Geophys. Res.*, *109*, D11201, doi:10.1029/2003JD004232.

Koons, H. C., and J. L. Roeder (1990), A survey of equatorial magnetospheric wave activity between 5 and 8 R_E, *Planet. Space Sci.*, *38*, 1335, doi:10.1016/0032-0633(90)90136-E.

Lam, M. M., R. B. Horne, N. P. Meredith, and S. A. Glauert (2007), Modeling the effects of radial diffusion and plasmaspheric hiss on outer radiation belt electrons, *Geophys. Res. Lett.*, *34*, L20112, doi:10.1029/2007GL031598.

Larsen, T. R., J. B. Reagan, W. L. Imhof, L. E. Montbriand, and J. S. Belrose (1976), A coordinated study of energetic electron precipitation and D region electron concentrations over Ottawa during disturbed conditions, *J. Geophys. Res.*, *81*, 2200, doi:10.1029/JA081i013p02200.

Lastovicka, J. (1996), Effects of geomagnetic storms in the lower ionosphere, middle atmosphere and troposphere, *J. Atmos. Terr. Phys.*, *58*, 831, doi:10.1016/0021-9169(95)00106-9.

Lauben, D. S., U. S. Inan, and T. F. Bell (2001), Precipitation of radiation belt electrons induced by obliquely propagating lightning-generated whistlers, *J. Geophys. Res.*, *106*, 29,745, doi:10.1029/1999JA000155.

Lawrence, D J., M. F. Thomsen, J. E. Borovsky, and D. J. McComas (1999), Measurements of early and late-time plasmasphere refilling as observed from geosynchronous orbit, *J. Geophys. Res.*, *104*, 14,691, doi:10.1029/1998JA900087.

Lezniak, T. W., R. L. Arnoldy, G. K. Parks, and J. R. Winkler (1968), Measurements and intensity of energetic electrons at the equator at 6.6 R_E, *Radio Sci.*, *3*, 710.

Li, X., D. N. Baker, M. Temerin, T. E. Cayton, E. G. D. Reeves, R. A. Christensen, J. B. Blake, M. D. Looper, R. Nakamura, and S. G. Kanekal (1997), Multispacecraft observations of the outer zone electron variation during the November 3–4, 1993, magnetic storm, *J. Geophys. Res.*, *102*, 14,123, doi:10.1029/97JA01101.

Lorentzen, K. R., M. P. McCarthy, G. K. Parks, J. E. Foat, R. M. Millan, D. M. Smith, R. P. Lin, and J. P. Treilhou (2000), Precipitation of relativistic electrons by interaction with electromagnetic ion cyclotron waves, *J. Geophys. Res.*, *105*, 5381, doi:10.1029/1999JA000283.

Lyons, L. R., R. M. Thorne, and C. F. Kennel (1972), Pitch-angle diffusion of radiation belt electrons within the plasmasphere, *J. Geophys. Res.*, *77*, 3455, doi:10.1029/JA077i019p03455.

Madden, D., and M. S. Gussenhoven (1990), Auroral Boundary Index from 1983 to 1990, *Tech. Rep. GL-TR-90-0358*, Air Force Geophys. Lab., Hanscom Air Force Base, Mass, 21 Dec.

Meredith, N. P., R. B. Horne, R. H. A. Iles, R. M. Thorne, D. Heynderickx, and R. R. Anderson (2002), Outer zone relativistic electron acceleration associated with substorm-enhanced whistler mode chorus, *J. Geophys. Res.*, *107*(A7), 1144, doi:10.1029/2001JA900146.

Meredith, N. P., R. B. Horne, S. A. Glaurt, R. M. Thorne, D. Summers, J. M. Albert, and R. R. Anderson (2006), Energetic outer zone electron loss timescales during low geomagnetic activity, *J. Geophys. Res.*, *111*, A05212, doi:10.1029/2005JA011516.

Moldwin, M. B., M. F. Thomsen, S. J. Bame, D. J. McComas, and K. R. Moore (1994), An examination of the structure and dynamics of the outer plasmasphere using multiple geosynchronous satellites, *J. Geophys. Res.*, *99*, 11,475, doi:10.1029/93JA03526.

Pfitzer, K. A., and J. R. Winckler (1968), Experimental observations of a large addition to the electron inner radiation belt after a solar flare event, *J. Geophys. Res.*, *73*, 5792, doi:10.1029/JA073i017p05792.

Randall, C. E., V. L. Harvey, C. S. Singleton, S. M. Bailey, P. F. Bernath, M. Codrescu, H. Nakajima, and J. M. Russell (2007), Energetic particle precipitation effects on the Southern Hemisphere stratosphere in 1992–2005, *J. Geophys. Res.*, *112*, D08308, doi:10.1029/2006JD007696.

Rees, M. H. (1963), Auroral ionization and excitation by incident energetic electrons, *Planet. Space Sci.*, *11*, 1209, doi:10.1016/0032-0633(63)90252-6.

Rees, M. H. (1964), Note on the penetration of energetic electrons into the Earth's atmosphere, *Planet. Space Sci.*, *12*, 722, doi:10.1016/0032-0633(64)90236-3.

Rodger, C. J., M. A. Clilverd, and R. J. McCormick (2003), Significance of lightning-generated whistlers to inner radiation belt electron lifetimes, *J. Geophys. Res.*, *108*(A12), 1462, doi:10.1029/2003JA009906.

Rodger, C. J., M. A. Clilverd, N. R. Thomson, R. J. Gable, A. Seppala, E. Turuned, N. P. Meredith, M. Parrot, J.-A. Sauvaud, and J.-J. Berthelier (2007), Radiation belt electron precipitation into the atmosphere: Recovery from a geomagnetic storm, *J. Geophys. Res.*, *112*, A11307, doi:10.1029/2007JA012383.

Rozanov, E., L. Callis, M. Schlesinger, F. Yang, N. Andronova, and V. Zubov (2005), Atmospheric response to NO_y source due to energetic electron precipitation, *Geophys. Res. Lett.*, *32*, L14811, doi:10.1029/2005GL023041.

Sandel, B. R., and M. H. Denton (2007), Global view of refilling of the plasmasphere, *Geophys. Res. Lett.*, *34*, L17102, doi:10.1029/2007GL030669.

Seaton, M. J. (1954), Excitation processes in the aurora and airglow 1. Absolute intensities, relative ultra-violet intensities and electron densities in high latitude aurora, *J. Atmos. Terr. Phys.*, *4*, 285, doi:10.1016/0021-9169(54)90060-4.

Seki, K., Y. Miyoshi, D. Summers, and N. P. Meredith (2005), Comparative study of outer-zone relativistic electrons observed by Akebono and CRRES, *J. Geophys. Res.*, *110*, A02203, doi:10.1029/2004JA010655.

Selesnick, R. S. (2006), Source and loss rates of radiation belt relativistic electrons during magnetic storms, *J. Geophys. Res.*, *111*, A04210, doi:10.1029/2005JA011473.

Selesnick, R. S., J. B. Blake, and R. A. Mewaldt (2003), Atmospheric losses of radiation belt electrons, *J. Geophys. Res.*, *108*(A12), 1468, doi:10.1029/2003JA010160.

Sheldon, W. R., J. R. Benbrook, and G. J. Byrne (1988), The effect of mid-latitude electron precipitation on the geoelectric field, *J. Atmos. Terr. Phys.*, *50*, 1019, doi:10.1016/0021-9169(88)90090-6.

Shprits, Y. Y., and R. M. Thorne (2004), Time dependent radial diffusion modeling of relativistic electrons with realistic loss rates, *Geophys. Res. Lett.*, *31*, L08805, doi:10.1029/2004GL019591.

Shprits, Y. Y., R. M. Thorne, R. Friedel, G. D. Reeves, J. Fennell, D. N. Baker, and S. G. Kanekal (2006), Outward radial diffusion driven by losses at magnetopause, *J. Geophys. Res.*, *111*, A11214, doi:10.1029/2006JA011657.

Shprits, Y. Y., N. P. Meredith, and R. M. Thorne (2007), Parameterization of radiation belt electron loss timescales due to interactions with chorus waves, *Geophys. Res. Lett.*, *34*, L11110, doi:10.1029/2006GL029050.

Siskind, D. E. (2002), Comment on "Solar-atmospheric coupling by electrons (SOLACE), 3, Comparisons of simulations and observations 1979–1997, issues and implications" by Linwood B. Callis et al., *J. Geophys. Res.*, *107*(D22), 4633, doi:10.1029/2001JD001141.

Smith, E. J., A. M. A. Frandsen, B. T. Tsurutani, R. M. Thorne, and K. W. Chan (1974), Plasmaspheric hiss intensity variations during magnetic storms, *J. Geophys. Res.*, *79*, 2507, doi:10.1029/JA079i016p02507.

Sojka, J. J, and G. L. Wrenn (1985), Refilling of geosynchronous flux tubes as observed at the equator by GEOS 2, *J. Geophys. Res.*, *90*, 6379, doi:10.1029/JA090iA07p06379.

Su, Y.-J., M. F. Thomsen, J. E. Borovsky, and D. J. Lawrence (2001), A comprehensive survey of plasmasphere refilling at geosynchronous orbit, *J. Geophys. Res.*, *106*, 25,615.

Summers, D., and R. M. Thorne (2003), Relativistic electron pitch-angle scattering by electromagnetic ion cyclotron waves during geomagnetic storms, *J. Geophys. Res.*, *108*(A4), 1143, doi:10.1029/2002JA009489.

Summers, D., R. M. Thorne, and F. Xiao (1998), Relativistic theory of wave-particle resonant diffusion with application to electron acceleration in the magnetosphere, *J. Geophys. Res.*, *103*, 20,487.

Summers, D., C. Ma, and T. Mukai (2004), Competition between acceleration and loss mechanisms of relativistic electrons during geomagnetic storms, *J. Geophys. Res.*, *109*, A04221, doi:10.1029/2004JA010437.

Thomsen, M. F. (2004), Why *Kp* is such a good measure of magnetospheric convection, *Space Weather*, *2*, S11004, doi:10.1029/2004SW000089.

Thorne, R. M. (1997), Energetic radiation belt electron precipitation: A natural depletion mechanism for stratospheric ozone, *Science*, *195*, 287.

Thorne, R. M. (1980), The importance of energetic particle precipitation on the chemical composition of the middle atmosphere, *Pure Appl. Geophys.*, *118*, 128.

Thorne, R. M., T. P. O'Brien, Y. Y. Shprits, D. Summers, and R. B. Horne (2005), Timescale for MeV electron microburst loss during geomagnetic storms, *J. Geophys. Res.*, *110*, A09202, doi:10.1029/2004JA010882.

Tinsley, B. A., G. B. Burns, and L. Zhou (2007), The role of the global electric circuit in solar and internal forcing of clouds and climate, *Adv. Space Res.*, *40*, 1126.

Tsurutani, B. T., E. J. Smith, and R. M. Thorne (1975), Electromagnetic hiss and relativistic electron losses in the inner zone, *J. Geophys. Res.*, *80*, 600.

Voss, H. D., M. Walt, W. L. Imhof, J. Mobilia, and U. S. Inan (1998), Satellite observations of lightning-induced electron precipitation, *J. Geophys. Res.*, *103*, 11,725.

West, H. I., R. M. Buck, and J. R. Walton (1972), Shadowing of electron azimuthal-drift motions near the noon magnetopause, *Nature Phys. Sci.*, *240*, 6.

West, H. I., R. M. Buck, and G. T. Davidson (1981), The dynamics of energetic electrons in the Earth's outer radiation belt during 1968 as observed by the Lawrence Livermore National Laboratory's spectrometer on Ogo 5, *J. Geophys. Res.*, *86*, 2111.

_____

J. E. Borovsky, Los Alamos National Laboratory, Mail Stop D466, Los Alamos, NM 87545, USA. (jborovsky@lanl.gov)

M. H. Denton, Department of Communication Systems, Lancaster University, Lancaster LA1 4WA, UK.